energies

MDPI

Article

Numerical Study on Non-Uniform Temperature Distribution and Thermal Performance of Plate Heat Exchanger

Jeonggyun Ham [1], Gonghee Lee [2], Dong-wook Oh [1] and Honghyun Cho [1,*]

[1] Department of Mechanical Engineering, Graduate School of Chosun University, 309 Pilmundaero, Dong-gu, Gwangju 61452, Korea; orchiders@chosun.kr (J.H.); dwoh@Chosun.ac.kr (D.-w.O.)
[2] Regulatory Assessment Department, Korea Institute of Nuclear Safety, Daejeon 34142, Korea; k532lgh@kins.re.kr
* Correspondence: hhcho@chosun.ac.kr; Tel.: +82-62-230-7050; Fax: +82-62-230-7055

Abstract: In this study, computational fluid dynamics (CFD) analysis was performed to investigate the cause of the thermal stratification in the channel and the temperature non-uniformity of the plate heat exchanger. The flow velocity maldistribution of the channel and the merging parts caused temperature non-uniformity in the channel width direction. The non-uniformity of flow velocity and temperature in the channel is shown in Section 1 > Section 3 > Section 2 from the heat exchanger. The non-uniform temperature distribution in the channel caused channel stratification and non-uniform outlet temperature. Stratification occurred at the channel near the merging due to the flow rate non-uniformity in the channel. In particular, as the mass flow rate increased from 0.03 to 0.12 kg/s and the effectiveness increased from 0.436 to 0.615, the cold-side stratified volume decreased from 4.06 to 3.7 cm^3, and the temperature difference between the stratified area and the outlet decreased from 1.21 K to 0.61 K. The increase in mass flow and the decrease in temperature difference between the cold and hot sides alleviated the non-uniformity of the outlet temperature due to the increase in effectiveness. Besides, as the inlet temperature difference between the cold and the hot side increases, the temperature non-uniformity at the outlet port is poor due to the increase in the stratified region at the channel, and the distance to obtain a uniform temperature in the outlet pipe increases as the temperature at the hot side increases.

Keywords: plate heat exchanger; velocity distribution; non-uniformity; thermal performance; stratification

Citation: Ham, J.; Lee, G.; Oh, D.-w.; Cho, H. Numerical Study on Non-Uniform Temperature Distribution and Thermal Performance of Plate Heat Exchanger. *Energies* **2021**, *14*, 8280. https://doi.org/10.3390/en14248280

Academic Editor: Lyes Bennamoun

Received: 28 October 2021
Accepted: 18 November 2021
Published: 8 December 2021

1. Introduction

Recently, as energy reduction and greenhouse gas emission regulations are being strengthened worldwide, a lot of efforts such as wettability improvement effect [1,2], optimization of fin material, shape, arrangement [3–5], application of the nanofluid [6,7], using the nozzle for jet impingement heat transfer [8,9], using porous media [10], optimization of the flow distribution [11–14] are being implemented to improve the efficiency of heat exchangers. Payambarpour et al. [1,2] numerically confirmed the decrease in thermal efficiency as the locally wetted surface increased in the plate tube heat exchanger and noted that the concentrated pattern had higher thermal efficiency in the wetted region than the localized pattern. Kim [4] compared various optimized finned annuli with various fin shapes. The author reported that thermal performance improved in the order of straight-finned annuli, circular-sectored-finned annuli, finned annuli with linearly decreasing porosity, finned annuli with linearly increasing fin thickness, and finned annuli with variable fin thickness. Goodarzi et al. [6] reported an increased pumping power consumption of the plate heat exchanger due to the augmentation of Reynolds number or nanomaterial fraction. The heat transfer performance could be improved when aqueous nanofluids such as MWCNT (Multi-walled carbon nanotube), FMWCNT-Cys (Functionalized multi-wall carbon nanotube with cysteine), and FMWCNT-Ag (Functionalized multi-walled carbon nanotube with silver) were used as coolants.

To obtain the theoretical maximum efficiency in the heat exchanger, the temperature difference between the cold and hot sides must be continuously maintained in the countercurrent flow configuration [15]. However, the flow distribution for each channel is different according to the geometry of the heat exchanger, and the temperature distribution in the heat exchanger is also locally non-uniform. Because the plate heat exchanger has a higher heat exchange area and density than other heat exchangers, the flow distribution for each channel and the flow velocity distribution within the channel are very non-uniform. This problem is confirmed in various heat exchangers such as parallel flow compact heat exchangers, shell and tube heat exchangers, plate-fin heat exchangers, printed circuit heat exchangers.

In the heat exchanger, the decrease in heat transfer performance due to non-uniformity of flow distribution for each channel or location is due to inlet velocity distribution, flow configurations such as U-type (parallel flow) and Z-type (reverse flow), flow resistance, and header shape. About this problem, parallel flow heat exchangers studied the flow distribution of single-phase flow through experiments and analysis. They confirmed that the non-uniformity of flow distribution is caused by the jet flow generated when the flow is introduced from the inlet header to the distributor. The U-type flow configuration forms a more uniform flow distribution than the Z-type flow distribution. [11,12]. Moreover, to suppress the jet flow generated in the distributor and improve the pressure distribution in the header, the shape improvement of the distribution part (modification of the area and shape of each channel, addition of baffles, modification of the header design) was attempted. It succeeded in alleviating the unevenness of the flow distribution [11–14]. In particular, Said et al. [14] investigated whether flow rate uniformity could be confirmed by applying an orifice and nozzle to a compact parallel heat exchanger. They confirmed that the flow mal-distribution decreased 12 times when the orifice was applied while the pressure drop increased by 7.8%.

On the other hand, when the nozzle is applied, the flow mal-distribution is reduced by 7.8 times, and the pressure drop can be reduced by 9.8%. In the case of a shell and tube heat exchanger, research was conducted to improve the flow distribution non-uniformity through the shape of the header, the arrangement of the tube, and the use of the baffle. Labbadlia et al. [16] investigated the uniformity of flow distribution according to the tube arrangement of shell and tube. They reported that when the tube arrangement angle is 45°, the maximum flow rate can be confirmed in multiple pipes. In contrast, when the tube arrangement angle is 60°, a uniform flow rate distribution can be obtained. Wang et al. [17] reviewed the utility of the porous baffle and confirmed that the porous baffle reduced the mal-distribution by 1/3 compared to the prototype baffle. Kim et al. [18] considered using a multi-porous plate to ensure a uniform flow rate distribution of a heat exchanger used in a sodium-cooled fast reactor (SFR) steam generator. The improvement of flow uniformity and pressure drop through the use of multi-porous plates was confirmed through experiment and analysis.

Plate fin heat exchanger tried to improve the non-uniformity of flow distribution through porous baffles and improvement of the header shape. Wen et al. [19] confirmed that the non-uniformity of flow distribution of conventional heat exchangers used in industry is studied through the PIV (particle image velocimetry) technique of the plate heat exchanger, and it is confirmed that it is possible to improve the flow distribution of the plate-fin heat exchanger through the introduction of a porous baffle. Wang et al. [20] reported that two-phase flow distribution is more complex and non-uniform than single-phase flow distribution in the plate-fin heat exchanger. It was also mentioned that headers with porous baffles could effectively improve the two-phase flow distribution and are an essential factor in the design of plate-fin heat exchangers. Moreover, Zang et al. [21] and Yang et al. [22] reported that it is possible to get a more uniform flow distribution of plate-fin heat exchangers and improve heat exchange performance by improving header shape through CFD analysis.

Studies on the non-uniformity of flow distribution in plate heat exchangers have mainly been indirectly verified by measuring the temperature distribution in the outer channel through a thermal imaging camera [23–25], and it was investigated by flow maldistribution parameter [26,27], a parameter based on the friction coefficient of the port and channel shape. Jin and Hrnjak [23] investigated the effect of the heat transfer plate at the end of the plate heat exchanger. If the number of channels in the plate heat exchanger is small, the end-plate acts as a fin and causes heat loss, and the effect is that the number of channels increases, the effect weakens accordingly. Navarro-Peris et al. [24,25] confirmed the non-uniform heat distribution of a brazed plate heat exchanger for an evaporator with a thermal imaging camera. It was confirmed that the evaporation temperature decreased, and a significant portion of the liquid was accumulated in the end channel of the evaporator, which was caused by poor refrigerant distribution.

Since the flow composition of the plate heat exchanger also affects the performance of the heat exchanger, this study was conducted. Rao and Das [28] experimentally investigated the influence of flow maldistribution according to the Z- and U-type flow composition of a plate heat exchanger. They reported that flow maldistribution of Z-type is more severe than that of U-type, and flow maldistribution is the flow velocity. It was confirmed to have a correlation with the number of channels and port size. Tereda et al. [29] reported that because the flow maldistribution of a plate heat exchanger is greatly affected by the size of the header and flow rate, it is necessary to supplement the design method of the plate heat exchanger considering the pre-existing uniform flow distribution. In addition, another study by Rao and Das [30] investigated the relationship between flow rate uniformity and heat exchange performance of a multi-pass plate heat exchanger. Increasing the flow maldistribution parameter degrades the performance of the plate heat exchanger. In the case of a plate heat exchanger with multiple passes, it was confirmed that the decrease in thermal performance of the plate heat exchanger due to an increase in flow maldistribution parameter was slighter than that of a plate heat exchanger with a single-pass. Bobbili et al. [26] confirmed that the increase in the number of heat plates increases the difference in pressure and velocity distribution through an experiment in a plate heat exchanger, thereby causing an increase in the flow maldistribution parameter. In addition, Brenk et al. [31] proposed a methodology for modifying a 3D shape into a 2D shape to evaluate the maldistribution of a plate heat exchanger.

The thermal performance of the plate heat exchanger is easily affected by the local dead zone or maldistribution of the flow rate because the plate heat exchanger is more compact than other heat exchangers. Poor flow distribution within the channel causes local overheating or overcooling. It creates a temperature difference for countercurrent heat exchange and causes non-uniformity of the temperature at the outlet. Moreover, these phenomena can cause a problem that can underestimate or overestimate the thermal performance of heat exchangers. This problem is more prominent as the size of the plate heat exchanger increases. It is essential to understand the plate heat exchanger characteristics and minimalize uncertainty on measuring thermal performance in the plate heat exchanger because it is widely used in industrial fields and for various purposes. In addition, incorrect performance measurement can cause serious problems in the temperature management of critical energy equipment. Therefore, in this study, the temperature distribution and thermal stratification phenomena at the channel of the plate heat exchanger were numerically investigated. In addition, the relationship between the non-uniformity of the outlet temperature and the operating conditions of the plate heat exchanger was analyzed. This study makes it possible to reduce errors in performance prediction due to the maldistribution of the flow rate in a large plate heat exchanger and contribute to accurate performance evaluation through proper temperature measurement at the outlet of the heat exchanger.

2. Simulation Method

2.1. Governing Equation

For the analysis of heat and flow of the plate heat exchanger, it is assumed that the fluid flowing in the plate heat exchanger is an incompressible fluid, and the flow of the fluid is a single-phase flow and a three-dimensional steady-state. Furthermore, heat loss from the outer wall of the plate heat exchanger was neglected. Therefore, the continuity, momentum, and energy equations used for thermal and flow analysis are shown in Equations (1)–(3).

$$\frac{\partial(\rho\overline{u}_i)}{\partial x_i} = 0 \tag{1}$$

$$u_j\frac{\partial(\rho\overline{u}_i)}{\partial x_i} = \frac{\partial p}{\partial x_i} + \frac{\partial}{\partial x_i}\left((\mu+\mu_t)\cdot\frac{\partial\overline{u}_i}{\partial x_j}\right) \tag{2}$$

$$c_p\cdot u_j\frac{\partial(\rho\cdot T)}{\partial x_j} = \frac{\partial}{\partial x_j}\left((k+k_t)\cdot\frac{\partial\kappa}{\partial x_i}\right) \tag{3}$$

In general, $k-\omega$ SST, RNG $k-\varepsilon$, Standard $k-\varepsilon$, and Realizable $k-\varepsilon$ models are used for thermal and flow analysis of plate heat exchangers. The wide width, narrow channel height, and complex shape of the plate heat exchanger make it difficult to calculate the shear stress and velocity profile at the wall. Since the velocity profile in the vicinity of the wall depends on the shear stress, it is important to select a turbulence model. In particular, the calculation of wall shear stress is important because plate heat exchangers have complex curvature shapes and narrow channels. The turbulence model mainly used for CFD analysis of plate heat exchangers is divided into the $k-\omega$ SST and $k-\omega$ model group. The $k-\omega$ SST model interprets the vicinity layer near the wall, while the $k-\omega$ model interprets the boundary layer away from the wall. However, the SST model easily analyzes the lower viscous layer but requires high resolution on the wall and is suitable for free shear flow with stalactite-shaped pressure gradients. On the other hand, the RNG $k-\varepsilon$ model more accurately represents the flow with a strong shear region among the $k-\varepsilon$ model groups and has the advantage of requiring a lower resolution near the wall than the $k-\omega$ SST model. The analysis capacity load is small. In addition, it is suitable as a turbulence model for plate heat exchanger analysis because it is excellent in predicting turbulent anisotropy such as strong streamline curvature, swirling flow, or strong recirculating flow when RNG and enhanced wall function are used [32]. In general, the turbulence energy and its diffusion rate of the RNG $k-\varepsilon$ model are expressed by Equations (4) and (5).

$$\frac{\partial}{\partial t}(\rho k) + \frac{\partial}{\partial x_i}(\rho k u_i) = \frac{\partial}{\partial x_j}\left[\left(\mu+\frac{\mu_t}{\sigma_k}\right)\frac{\partial k}{\partial x_j}\right] + P_k - \rho\varepsilon \tag{4}$$

$$\frac{\partial}{\partial t}(\rho\varepsilon) + \frac{\partial}{\partial x_i}(\rho\varepsilon u_i) = \frac{\partial}{\partial x_j}\left[\left(\mu+\frac{\mu_t}{\sigma_k}\right)\frac{\partial\varepsilon}{\partial x_j}\right] + C_{1\varepsilon}\frac{\varepsilon}{k}P_k - C_{2\varepsilon}^{*}\rho\frac{\varepsilon^2}{k} \tag{5}$$

Here, $C_{2\varepsilon}^{*} = C_{2\varepsilon} + \frac{C_\mu\eta^3(1-\eta/\eta_0)}{1+\beta\eta^3}$ and $\eta = Sk/\varepsilon$.

To solve the momentum and energy equations, the SIMPLE (Semi-implicit method for pressure-linked equations) algorithm was used for pressure velocity coupling processing. PRESTO (pressure staggering option) was used for pressure calculation, and the remaining momentum, turbulence energy, turbulence energy diffusion rate, and energy equation were calculated in secondary order. If the residual for energy was 10^{-6}, and the remaining residuals were less than or equal to 10^{-4}, it was considered that convergence was reached.

2.2. Boundary and Simulation Condition

In this study, the analysis was conducted considering the influence of the mass flow rate of the working fluid and the inlet temperature difference between the cold and hot sides. Each inlet has a velocity inlet condition, and the outlet is set as a pressure outlet. The inlet and outlet turbulence intensities are equal to Equation (6).

$$I = 0.16\mathrm{Re}^{-1/8} \tag{6}$$

Table 1 shows the analysis conditions of this study.

Table 1. Simulation conditions of plate heat exchanger.

Contents	Cold Side		Hot Side	
	Mass Flow Rate (kg/s)	$T_{c,i}$ (K)	Mass Flow Rate (kg/s)	$T_{h,i}$ (K)
Mass flow rate	0.03–0.15	293.15	0.03	313.15
Temperature difference between cold and hot side	0.15	283.15–298.15	0.03	313.15

In the analysis, changes in the physical properties of water, which are fluids on the cold and hot sides, according to the temperature, were reflected. The density, specific heat, thermal conductivity, and water viscosity are shown in Equations (7)–(10) [33].

$$\rho(T) = -0.0035T^2 + 1.8142T + 765.33 \tag{7}$$

$$c_p(T) = 1.857 \times 10^{-6}T^4 - 0.00248T^3 + 1.25T^2 - 281.7T + 28070 \tag{8}$$

$$\mu(T) = -2.244 \times 10^{-9}T^3 + 2.344 \times 10^{-6}T^2 - 8.2 \times 10^{-3}T + 0.0967 \tag{9}$$

$$\mu(T) = -2.244 \times 10^{-9}T^3 + 2.344 \times 10^{-6}T^2 - 8.2 \times 10^{-3}T + 0.0967 \tag{10}$$

2.3. Geometry Modeling

Figure 1a,b shows the 3D modeling and the schematics of the plate heat exchanger. The simulation model of the plate heat exchanger consists of the cold and hot side channels, one heat transfer plate, and pipes of the cold and hot side. The geometry of the plate heat exchanger used in the study and Gulenoglu et al. [34] are the same. The chevron angle, height (β), and bending depth (b), which are the main design parameters of the plate heat exchanger, are 30° and 0.00276 m, respectively, and the length and diameter of the port and port of the plate heat exchanger are 0.335 m and 0.035 m. The shape of the plate heat exchanger used in the analysis was modeled using CAE software CATIA.

2.4. Data Analysis

The heat exchange amount of the plate heat exchanger was calculated by Equation (11).

$$Q = \dot{m}_c c_{p,c}(T_{c,o} - T_{c,i}) = \dot{m}_h c_{p,h}(T_{h,i} - T_{h,o}) \tag{11}$$

where $c_{p,c}$ and $c_{p,h}$ are the specific heats of the cold and hot side fluid. They are calculated based on the bulk temperature. Moreover, the convective heat transfer coefficient of the fluid is calculated by Equation (12).

$$h_c = \frac{Q}{A(T_{w,c} - T_{c,b})} \tag{12}$$

where $T_{c,b}$ and $T_{w,c}$ are the bulk and wall temperatures of the temperature of the cold side. The Nusselt number is defined by Equation (13).

$$Nu = \frac{h_c d_h}{k} \tag{13}$$

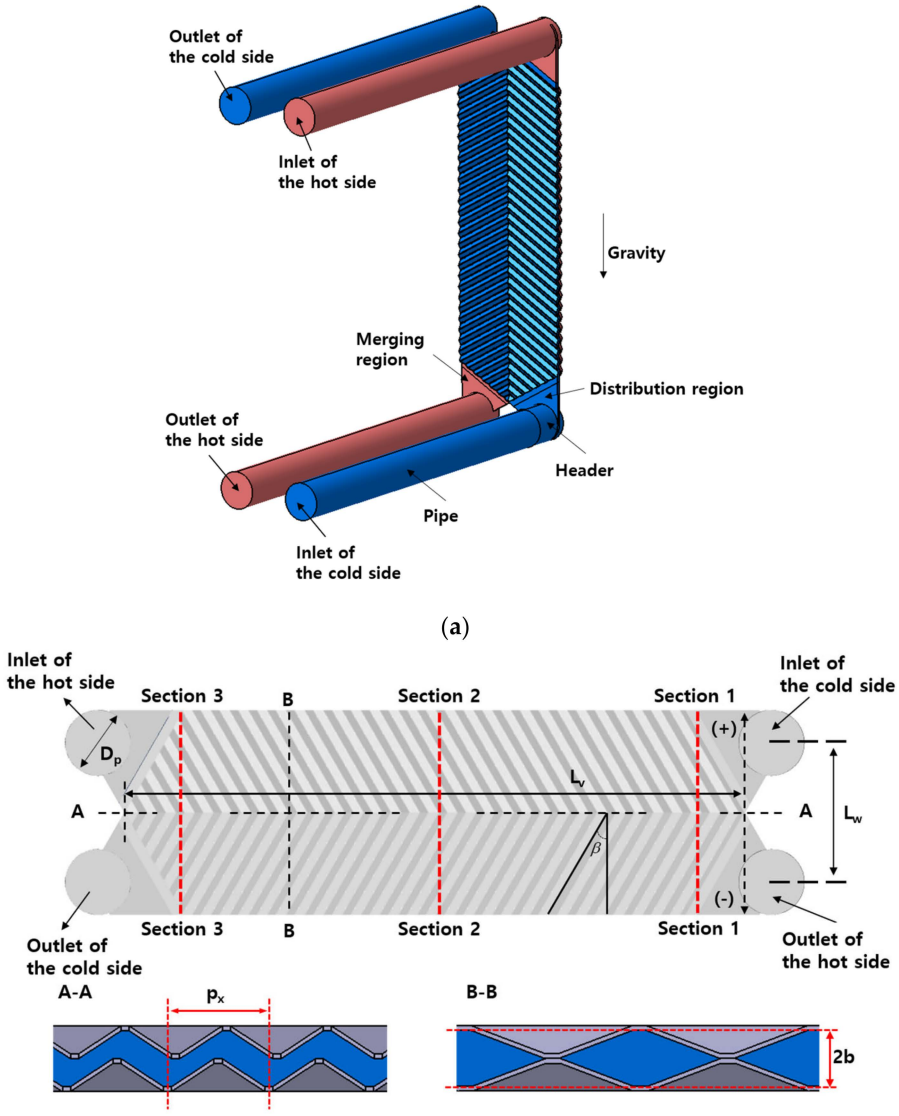

Figure 1. 3D modeling and schematics of the plate heat exchanger (PHX): (**a**) 3D modeling, and (**b**) schematics of PHX.

Equation (14) shows the effectiveness of the plate heat exchanger.

$$\varepsilon = \frac{Q_{avg}}{Q_{\max}} = \frac{m_c c_{p,c}(T_{c,o} - T_{c,i})}{C_{\min}(T_{h,i} - T_{c,i})} = \frac{m_h c_{p,h}(T_{h,i} - T_{h,o})}{C_{\min}(T_{h,i} - T_{c,i})} \tag{14}$$

Q_{max} is the maximum heat exchange amount that can be exchanged between the cold and hot sides, and C_{min} is the minimum heat capacity, which is expressed as Equation (15).

$$C_{\min} = \begin{cases} C_c = \dot{m}_c c_{p,c}\,, & C_c < C_h \\ C_h = \dot{m}_h c_{p,h}\,, & C_h < C_c \end{cases} \tag{15}$$

As shown in Figure 1, in the plate heat exchanger, the point where the distribution of the distribution ends (Section 1), the center of the heat exchanger where effective heat transfer occurs (Section 2), and the point where the distribution of the fluid occurs in the merged section (Section 3) are reflected to calculate channel flow rate and temperature

non-uniformity. The non-uniformity of the flow rate and temperature of the channel was calculated by Equation (16).

$$\phi = \sqrt{\frac{\sum_{i=1}^{N} \left(\beta_i - \overline{\beta}\right)^2}{N}} \tag{16}$$

where, $\overline{\beta}$ is the average ratio of the velocity or temperature, which can be calculated by Equation (17), and $\overline{\beta_i}$ is the flow rate or temperature ratio, which is defined by Equation (18).

$$\overline{\beta} = \frac{\left(\sum_{i=1}^{N} \beta_i\right)}{N} \tag{17}$$

$$\beta_i = V_i / V_{avg} \quad or \quad \beta_i = T_i / T_{avg} \tag{18}$$

2.5. Mesh Topology and Validation

Figure 2 shows generated mesh of the plate heat exchanger and the results of the grid independence test. The area in the heat exchange between the channels on the cold and hot side was designed using a polyhedral cell, and the inlet/outlet piping was designed with a prism/hex cell. Tetrahedral cells can maintain mesh quality even in complex shapes, but they require many cells and disadvantages of numerical diffusion. Polyhedral cells can approximate the gradient better because there are multiple cells adjacent to each cell compared to tetrahedral mesh. Polyhedral cells are also more sensitive to stretching than tetrahedral. In addition, polyhedral mesh requires fewer cells than tetrahedral mesh to secure analysis accuracy; thus, it is suitable for analyzing plate heat exchangers with complex curved shapes [35]. To describe the full development region, prism cells are located near the wall, and the first grid from the wall is located at $1 < y+ < 5$. The grid independence test is carried out within a grid number of 18,508,954 to 73,757,890. The outlet temperature and the pressure drop of the cold side are close to about 296.1 K and 21.1 kPa when the grid number is 47,423,034. The outlet temperature and the pressure drop of the cold side are no significant changes over the grid number of 47,423,034. Therefore, a model with a grid number of 47,423,034 is used in this study.

Figure 3 shows the comparison between the Nusselt correlation equation of Gulenoglu et al. [34], experimented on a plate heat exchanger of the same geometry, and the Nusselt number on the cold side calculated from the analysis results obtained in this study. When the inlet temperature of the cold side was 293.15 K, the Nusselt number calculated based on the analysis results of this study increased from 41.16 to 98.81 as the cold side mass flow increased from 0.03 kg/s to 0.12 kg/s. Compared with the Nusselt number correlation of Gulenoglu et al. [34], the error rate of the Nusselt number was 2.3–6.6%. Moreover, when the mass flow rate of the cold side was 0.09 kg/s, and the inlet temperature of the cold side increased from 283.15 K to 298.15 K, the Nusselt number increased from 78.7 to 85, and the error rate was 3.3–6% for these conditions. The Friction factor decreases from 1.984 to 1.348 as the mass flow rate of the cold side increases from 0.03 kg/s to 0.12 kg/s, and its error rate is 4–7.3%. Besides, the Friction factor decreases from 1.559 to 1.428 as the inlet temperature of the cold side increases from 283.15 K to 298.15 K, and its error rate is 4.8–6.8%. The experimental uncertainty about the Nusselt number and Friction factor of Gulenoglu et al. [34] was ±12.4% and ±11.8%, respectively. The deviation from the Nusselt number of Gulenoglu et al. [34] was 2.87%. Therefore, it can be judged that this simulation study properly predicts the experimental results.

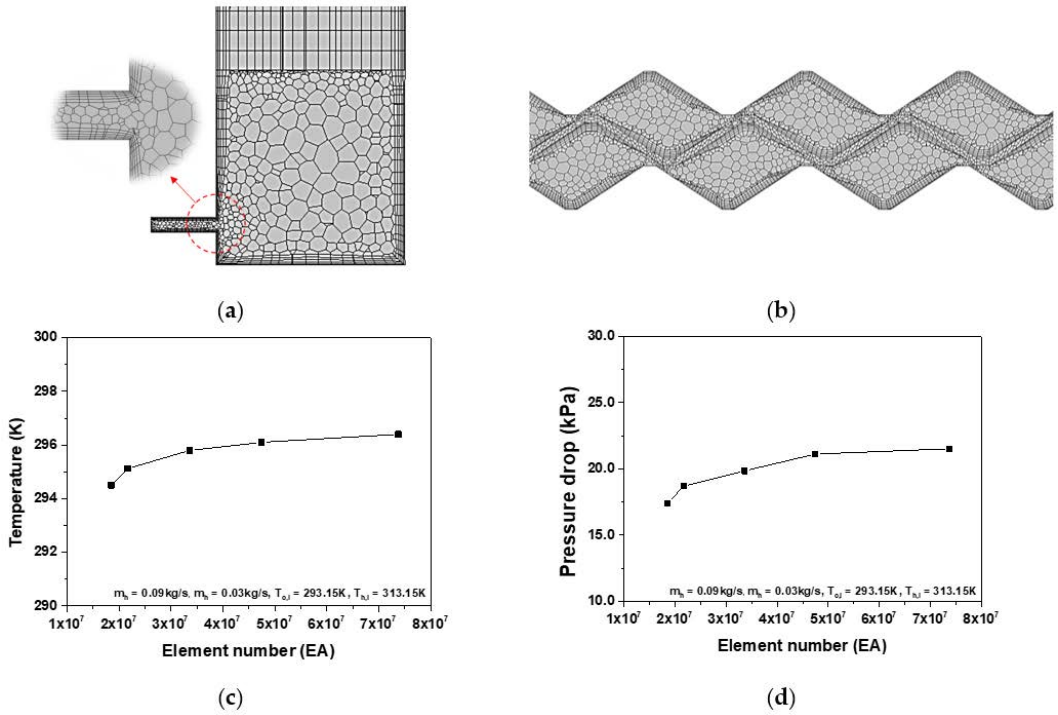

Figure 2. Comparison of Nusselt number according to mass flow rate and temperature: (**a**) Nusselt number according to the mass flow rate, (**b**) the Nusselt number according to the inlet temperature of the cold side; (**c**) friction factor according to the mass flow rate; (d) friction factor according to the inlet temperature.

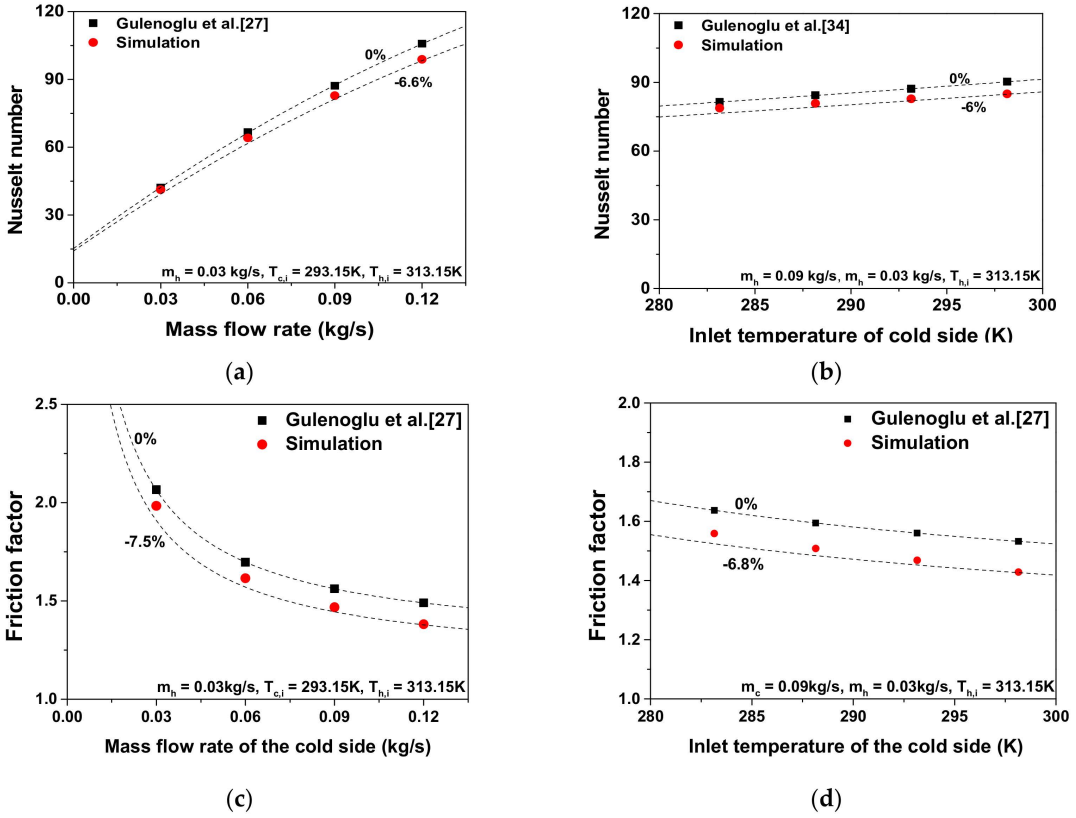

Figure 3. Comparison of Nusselt number according to mass flow rate and temperature: (**a**) Nusselt number according to the mass flow rate; (**b**) the Nusselt number according to the inlet temperature of the cold side; (**c**) friction factor according to the mass flow rate; (**d**) friction factor according to the inlet temperature.

3. Results and Discussion

3.1. Thermal Performance of PHX

Figure 4 shows the amount of heat transfer and effectiveness of the plate heat exchanger according to the change in the mass flow rate and the inlet temperature of the cold side. The amount of heat transfer increases from 1081 W to 1528 W in plate heat exchangers when the inlet temperatures of the hot and cold sides are constant at 283.15 K and 313.15 K, and the mass flow rate on the cold side increases from 0.03 kg/s to 0.12 kg/s. In addition, the effectiveness also increased from 0.436 to 0.615. An increase in the mass flow rate of the working fluid enhances convective heat transfer by intensifying the turbulence strength in the channel. Besides, thermal energy can be easily transferred because the mass flow rate difference between the cold and hot sides decreases the thermal capacity ratio. Therefore, it leads to an increase in the effectiveness of the plate heat exchanger. When the mass flow rates on the hot and cold sides are 0.03 kg/s and 0.09 kg/s, and the temperature of the hot side is 313.15 K when the inlet temperature of the cold side increases from 283.15 K to 298.15 K, the amount of the heat transfer decreases from 2147 W to 1111 W. The effectiveness slightly increased from 0.576 to 0.597. It is because, as the inlet temperature of the cold side increases, the amount of heat transfer decreases as the temperature difference between the cold and the hot side decreases; however, the increase in the overall heat transfer coefficient of the plate heat exchanger increases the effectiveness of the heat exchanger due to the increase in the flow rate in the channel of the cold side.

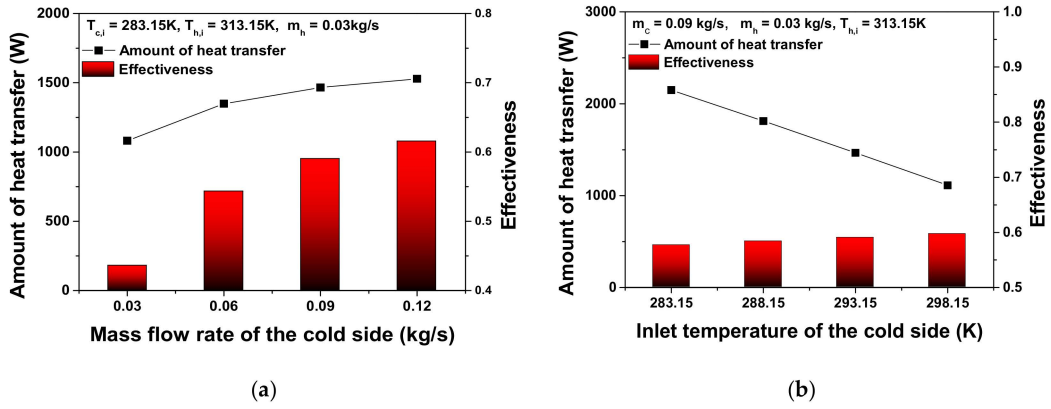

(**a**) (**b**)

Figure 4. Amount of heat transfer and effectiveness: (**a**) according to the mass flow rate of the cold side, (**b**) according to inlet temperature of the cold side.

3.2. Temperature and Velocity Distribution at the Channel of PHX

The channel of the plate heat exchanger consists of a distribution part, a heat exchange part, and a merging part, and the difference in velocity distribution of each channel in the distribution part affects the local heat transfer performance and causes thermal non-uniformity. Figure 5 shows the temperature distribution at the cold and hot side channels. The temperature distribution of the plate heat exchanger shows symmetry at the center of the channel. Both the cold and hot side channels have a symmetrical temperature distribution in the middle of the channel. However, it can be confirmed that the temperature distribution is non-uniform near the inlet and outlet ports. The channel of the cold side had a low temperature near the inlet port at the same flow direction length but had a relatively high temperature near the outlet port of the hot side channel. However, the temperature distribution was eccentric near the outlet ports of the cold and hot sides owing to the different velocity distribution at the channel.

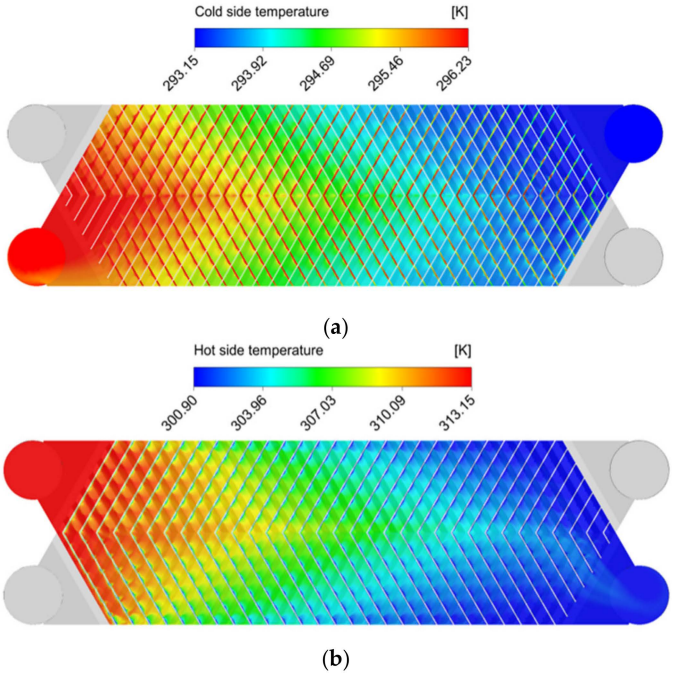

Figure 5. Temperature distribution at channels: (**a**) cold side, (**b**) hot side.

Figure 6 shows the temperature distribution and non-uniformity by channel location on the widthwise wall of the plate heat exchanger. In Section 1, it was confirmed that the temperature distribution appeared to be low in the positive direction with the inlet port of the cold side but high in the negative direction adjacent to the outlet port of the hot side. On the other hand, Section 2, which is the middle of the channel, shows a high temperature at the center of the channel, and it can be seen that the temperature distribution shows left-right symmetry. Moreover, in Section 3, it was confirmed that the temperature distribution was formed low in the negative direction where the outlet port of the cold side is located. In contrast, the high temperature in the positive direction is adjacent to the inlet temperature of the hot side. The temperature non-uniformity in Sections 1 and 2 of the channels of the cold side decreased to 0.0061–0.0028 and 0.0041–0.0034 as the mass flow rate of the cold side increased from 0.03 kg/s to 0.12 kg/s, whereas the temperature non-uniformity in Section 3 was instead increased to 0.0054–0.0064. These results imply that the temperature non-uniformity of the channel wall is closely related to the flow velocity distribution due to the geometrical characteristics of the plate heat exchanger. The local maldistribution of the flow velocity can improve the local heat transfer in a channel with high heat capacity. However, it is difficult to effectively transfer heat because the heat capacity at a specific location increases, and the temperature distribution is non-uniform.

Figure 7 shows the flow velocity distribution in the width direction in the cold side channel. In Section 1 of the plate heat exchanger, the flow velocity in the width direction has a high flow velocity in the positive direction close to the inlet port. In contrast, the flow velocity significantly decreased as it proceeded in the negative direction. In addition, it was confirmed that as the mass flow rate of the working fluid increased, the difference between the flow velocity at the position adjacent to the port and the flow velocity at the position far from the port increased. However, in Section 2, it was confirmed that the flow rate appeared symmetrical regardless of the increase in the mass flow rate of the working fluid. In the case of Section 1, as the fluid flows from the distribution part to the effective heat transfer area, the flow resistance is different because the cross-sectional area changes, and the distance between the center of the port and any location in Section 1 changes. However, in Section 2, unlike in Section 1, the flow is fully developed, showing a uniform flow velocity distribution in the width direction. In the case of Section 3, the cross-sectional area changes rapidly as the fluid flows from the heat transfer zone to the

merge part. In Section 3, the distance from the outlet port varies according to the width and length, so the relatively close negative direction has a high flow rate, whereas the positive direction far from the outlet port has a low flow rate. In the plate heat exchanger, the flow rate non-uniformity was formed in Section 1 > Section 3 > Section 2. As the mass flow of the cold side rate increases from 0.03 kg/s to 0.12 kg/s, the non-uniformity of the flow rates in Sections 1–3 increases to 0.121–0.510, 0.084–0.332, and 0.121–0.466. In a plate heat exchanger, the non-uniformity of the flow rate by location affects the non-uniformity of the wall temperature of the plate heat exchanger. The drift of the flow rate affects the temperature change by increasing the mass flow rate and local heat capacity. In Section 1 and Section 3, it can be seen that the point with a high flow rate has a relatively high mass flow rate, so that the temperature change is small. On the other hand, in Section 2, which has a uniform flow velocity distribution, the temperature distribution has uniformity. Therefore, to solve this problem, it is necessary to secure the uniformity of the flow rate through the shape improvement of the distribution and merging parts of the channel.

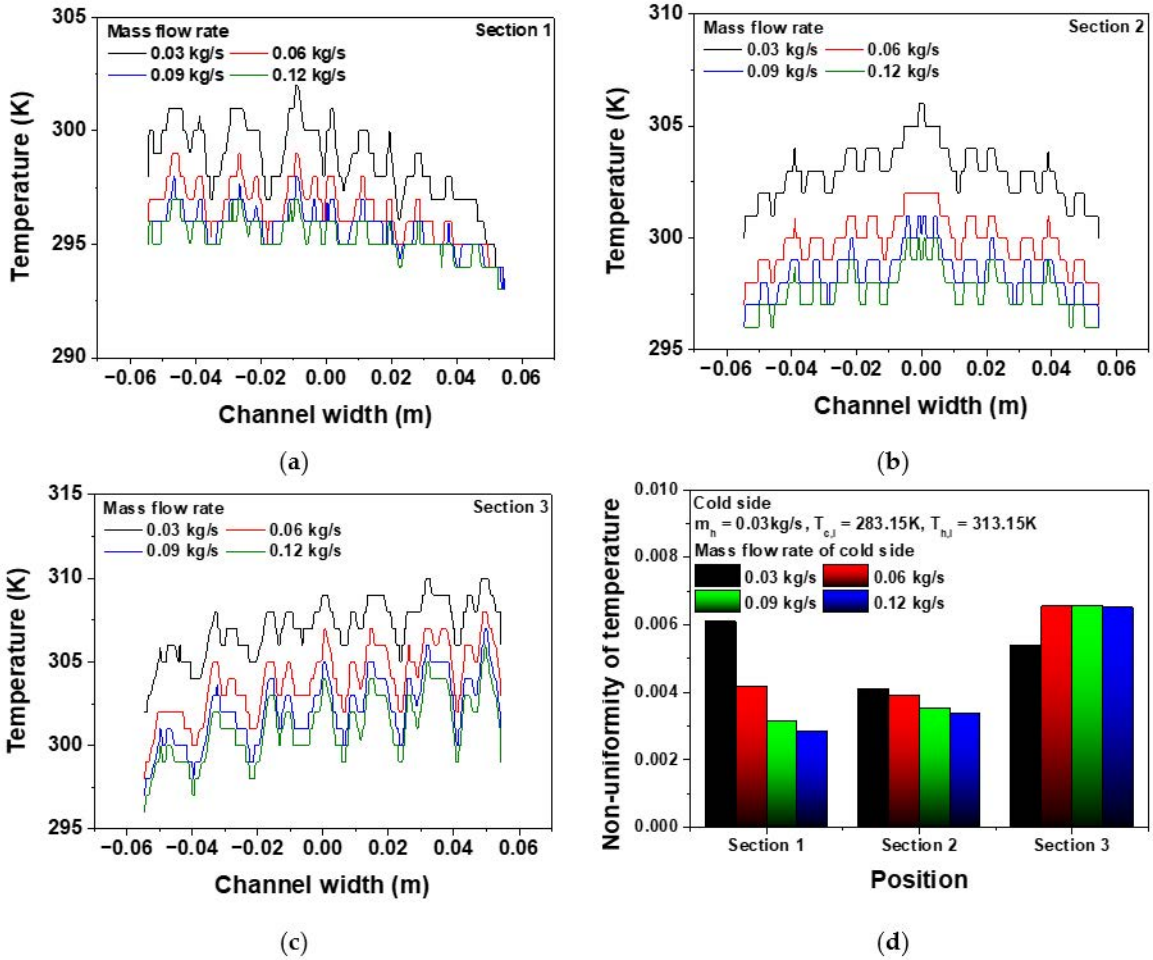

Figure 6. Cold side wall temperature: (**a**) Section 1, (**b**) Section 2, (**c**) Section 3, and (**d**) non-uniformity of temperature.

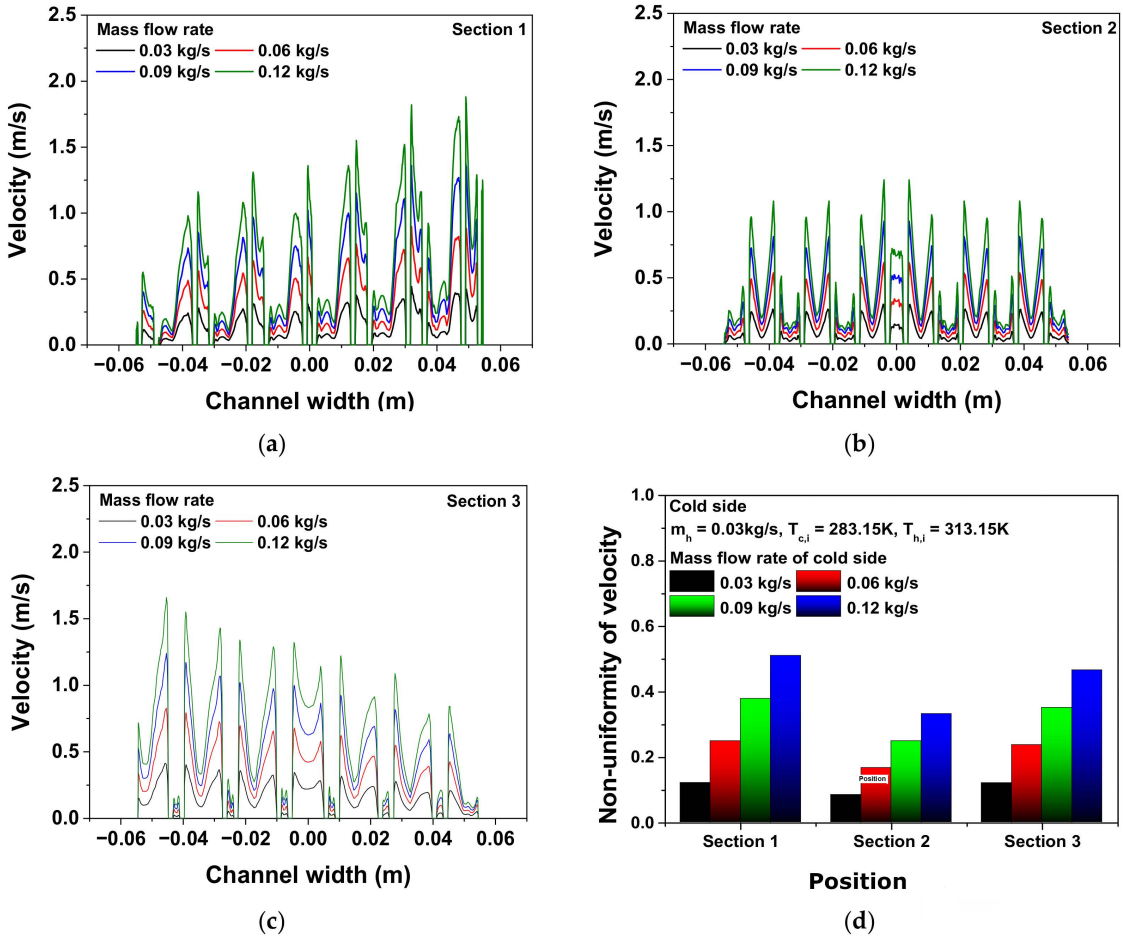

Figure 7. Velocity and cold side at each position: (**a**) Section 1, (**b**) Section 2, (**c**) Section 3, and (**d**) non-uniformity of velocity.

3.3. Non-Uniformity of Outlet Temperature in the PHX

Figure 8 shows the superheating region of the cold side channel and the subcooling region of the hot side channel. When the mass flow rates on the hot and cold sides are 0.03 kg/s and 0.09 kg/s, the inlet temperatures of the hot and cold sides are 293.15 K and 313.15 K. In the cold side channel, the area overheated above the outlet temperature was located in the center of the merging section. The area overheated than the outlet temperature in the hot side channel was located outside the converging section. This phenomenon is due to the non-uniformity of the flow velocity distribution locally in the plate heat exchanger channel. When the fluid flows from the merging part to the outlet port, the fluid does not mix and causes a stratified flow. Therefore, this phenomenon can be expressed as a part of the flow or thermal stratification, and in this study, it was defined as a stratification phenomenon. The stratification phenomenon in the channel is due to the non-uniformity of the flow velocity at the merge. The channel of the cold side has a relatively high heat transfer coefficient at a relatively high flow rate in the center of the distribution part and a low heat transfer coefficient in the side part. In addition, the local heat capacity is unbalanced due to the maldistribution of the mass flow rate. Although the heat transfer coefficient is locally increased due to the concentration of the flow rate, the heat capacity also increases. Therefore, the temperature at the point where the flow velocity is slow changes more rapidly. Thermal stratification occurs by this mechanism due to the non-uniform flow velocity at the distribution and merging section of each channel in the plate heat exchanger.

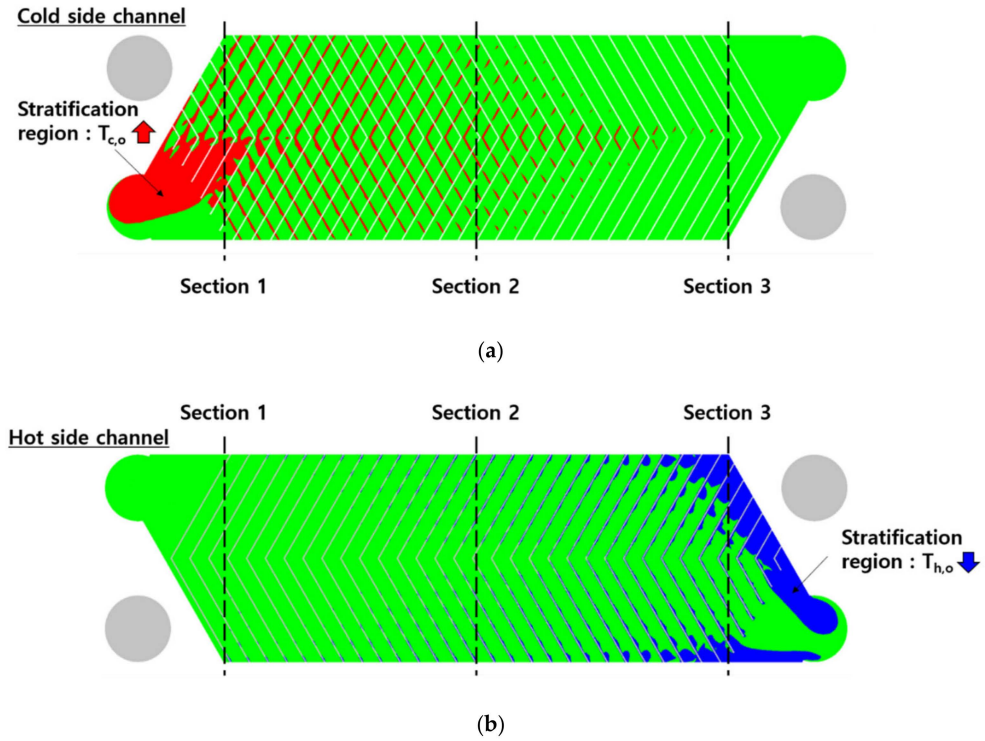

Figure 8. A subcooled region at the channel of the plate heat exchanger: (**a**) at cold side channel and (**b**) overheated region at the hot side.

Figure 9 shows the volume of the stratified region and the average temperature difference at the outlet, and the volume of the stratified region according to the change in availability. As the heat exchanger effectiveness increased from 0.436 to 0.615 due to an increase in the mass flow rate of the cold side, the stratified volume of the cold side-channel decreased from 4.056 cm^3 to 3.67 cm^3, while the stratified volume of the hot side-channel increased from 5.61 cm^3 to 6.02 cm^3. In addition, the average temperature of the stratified region and the temperature difference at the outlet decreased from 1.21 K to 0.61 K on the cold side. It decreased from 1.34 K to 1.23 K on the hot side. Due to the increase in the mass flow rate of the cold side, the heat capacity of the cold side increased, and the locally low convective heat transfer coefficient was improved. The increase in effectiveness in the heat exchanger reduces the stratified volume for each channel. As the inlet temperature of the cold side decreases from 303.15 K to 283.15 K, the effectiveness increases from 0.576 to 0.597, and the stratified volume of the cold side changes from 3.73 cm^3 to 3.64 cm^3. The stratified volume of the hot side also decreased slightly from 6.13 cm^3 to 5.97 cm^3. As the inlet temperature of the cold side decreased from 303.15 K to 283.15 K, the effectiveness increased from 0.576 to 0.597. Therefore, the stratified volume of the cold side decreases from 3.73 cm^3 to 3.64 cm^3, and the stratified volume of the hot side also slightly decreases from 6.13 cm^3 to 5.97 cm^3. Moreover, the difference between the average temperature and the outlet temperature of the stratified region at the cold and hot sides decreased from 1.18 K to 0.55 K and from 1.94 K to 0.92 K. The size of the stratified region varies depending on the operating conditions of the plate heat exchanger, which affects the non-uniformity of the outlet temperature.

The stratification phenomenon in the channel of the plate heat exchanger affects the non-uniformity of the outlet temperature. For heat exchanger performance evaluation, it is important to secure the uniformity of the outlet temperature. Figure 10 shows the difference between the maximum and minimum temperatures according to the dimensionless distance from the outlet port. In this study, the dimensionless distance is defined as the ratio of the outlet tube length to the tube diameter. As the mass flow rate of the cold side increases from 0.03 kg/s to 0.12 kg/s, the temperature at a point 1D away from the outlet

port decreases from 0.72 K to 0.54 K. However, as the dimensionless distance increases from 1D to 5D, the maximum and minimum temperature differences decrease. As the mass flow rate increases from 0.03 kg/s to 0.12 kg/s, it is confirmed that the difference between the maximum temperature and the minimum temperature in 5D is almost uniform within 0.12 K of the dimensionless distance. The difference in the inlet temperature of the plate heat exchanger increases the non-uniformity of the outlet temperature when the inlet temperature difference between the cold and hot sides increases from 15 K to 30 K, the difference between the maximum and minimum temperatures when the dimensionless distance was 1D increases from 0.41 K to 0.78 K. In addition, the difference between the maximum temperature and the minimum temperature is within 0.15 K when the dimensionless distance is 5D.

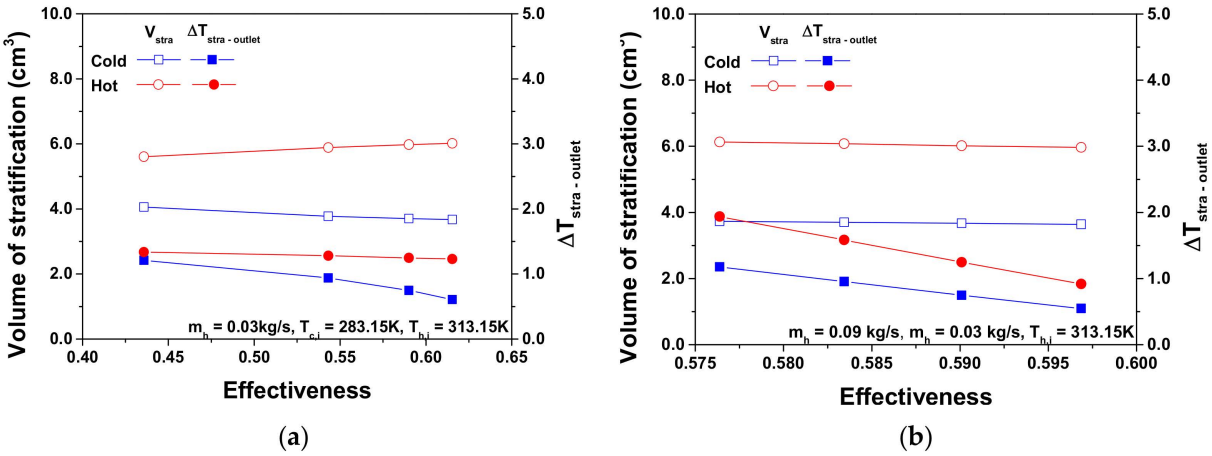

Figure 9. The volume of stratification and ΔT_(stra-outlet): (**a**) according to the mass flow rate of the cold side, (**b**) according to the inlet temperature of the cold side.

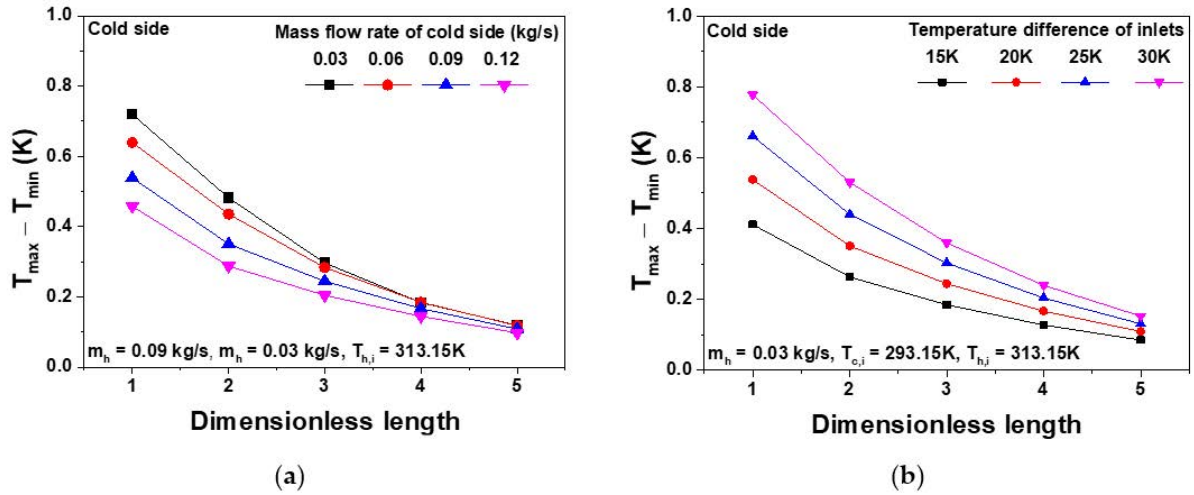

Figure 10. Maximum and minimum temperature difference according to a dimensionless length: (**a**) according to the mass flow rate of the cold side, (**b**) according to the inlet temperature.

Figure 11 shows the streamline and temperature distribution by location at the outlet port. When the fluid heat-exchanged in the channel flows into the outlet port from the channel merging part, the fluid does not diffuse due to a sudden change in cross-sectional area and forms a jet stream. For this reason, when the channel flows into the outlet port, the temperature inside the port forms a boundary layer and has an uneven temperature

distribution. However, the fluid colliding with the wall of the outlet port has rotational momentum and shows a vortex flow, and turbulent diffusion occurs. As the dimensionless distance increases, the non-uniform fluid mixes, and the temperature non-uniformity is reduced. In addition, the increase in the mass flow rate of the plate heat exchanger can enhance the rotational momentum at the outlet port, thereby further improving the temperature uniformity of the outlet port. On the other hand, when the inlet temperature difference between the cold and hot sides increases, the temperature non-uniformity of the fluid flowing into the outlet port increases, and the inlet distance which ensures temperature uniformity at the same mass flow rate is increased.

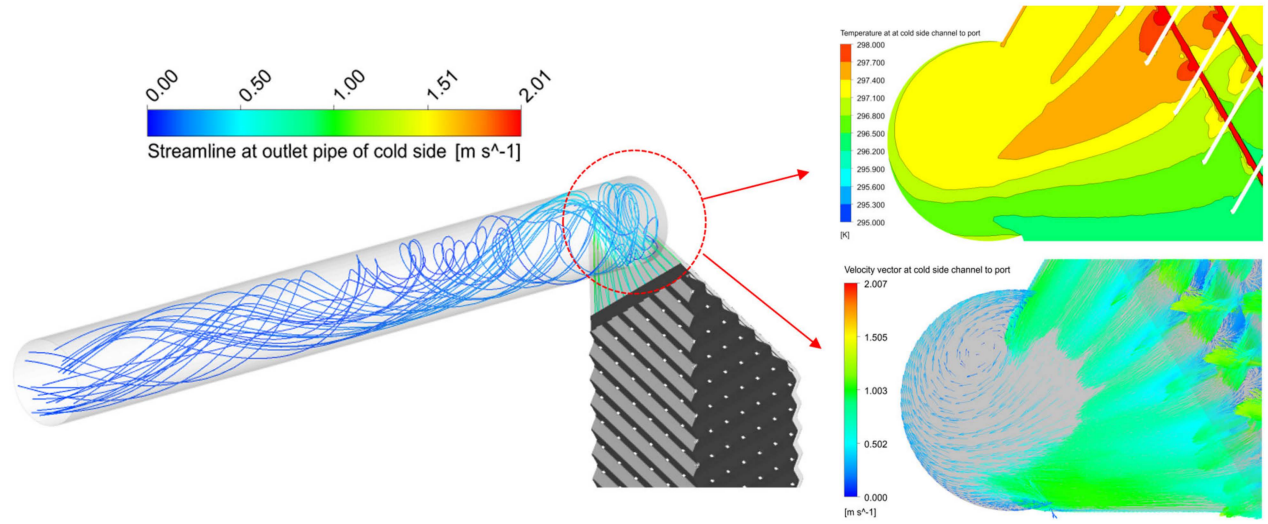

(**a**)

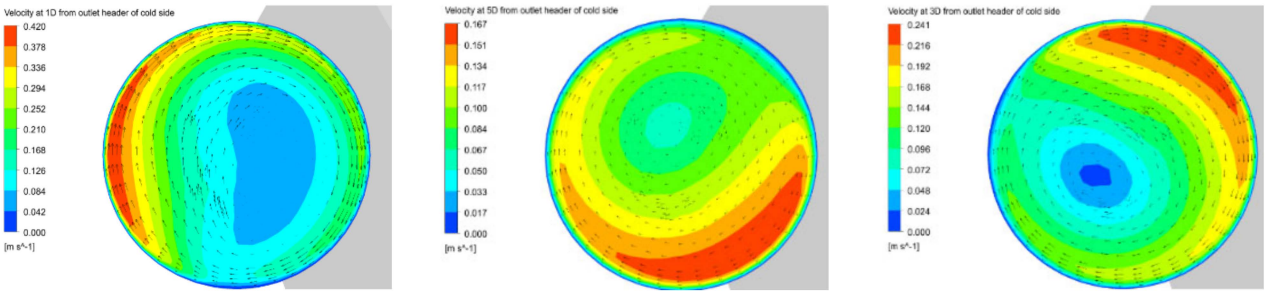

(**b1**) Lpipe/Dp = 1 (**b2**) Lpipe/Dp = 5 (**b3**) Lpipe/Dp = 3

(**b**)

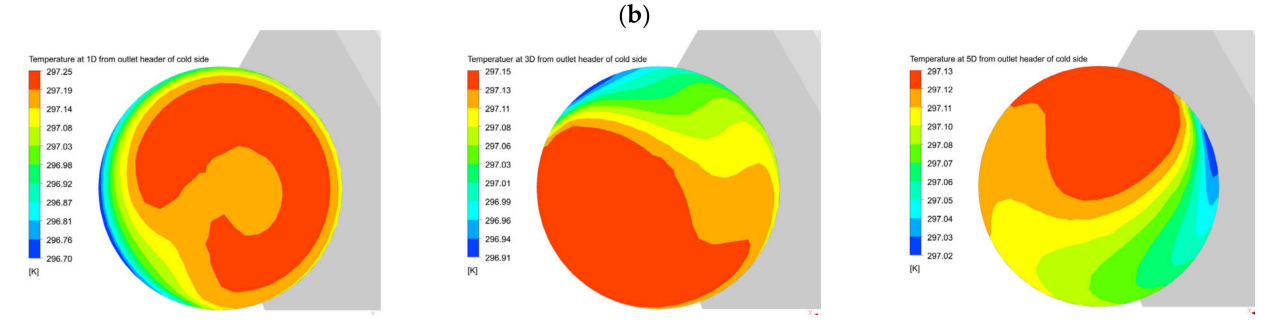

(**c1**) Lpipe/Dp = 1 (**c2**) Lpipe/Dp = 3 (**c3**) Lpipe/Dp = 5

(**c**)

Figure 11. Temperature and velocity distribution image at outlet port and pipe: (a) Streamline at the outlet port of cold side and temperature contour and velocity vector at the outlet port; (**b**) velocity contour and vector at the outlet pipe of the cold side; (**c**) temperature contour at the outlet pipe of the cold side.

4. Conclusions

The relationship between the non-uniformity of the outlet temperature and the operating conditions of the plate heat exchanger was investigated numerically in this study. As a result of the analysis, it was confirmed that the fluid temperature in the distribution and merging parts of the channel had non-uniformity in the width direction of the plate heat exchanger. The temperature in the channel is formed non-uniformly in the width direction due to the concentration of the flow velocity. The temperature non-uniformity in Sections 1 and 2 of the cold side-channel decreased to 0.0061–0.0028 and 0.0041–0.0034 as the cold side mass flow increased from 0.03 kg/s to 0.12 kg/s, whereas the temperature non-uniformity in Section 3 is rather increased to 0.0054–0.0064. The non-uniform temperature distribution in the plate heat exchanger is due to the flow velocity distribution in the channel. The flow rate non-uniformity in the channel was shown in the order of Section > 1 > Section 3 > Section 2. As the mass flow rate of the cold side increases from 0.03 kg/s to 0.12 kg/s, the flow velocity non-uniformities of Sections 1, 2, and 3 increased to 0.121–0.510, 0.084–0.332, and 0.121–0.466. The non-uniform flow velocity distribution in the channel generates a locally non-uniform heat capacity ratio and causes a stratification phenomenon in which local overheating or local subcooling occurs. As the mass flow rate of the cold side increased from 0.03 kg/s to 0.12 kg/s, the temperature non-uniformity in Section 1 decreased from 0.0061 to 0.0028. As the mass flow rate of the cold side increases from 0.03 kg/s to 0.12 kg/s, the effectiveness increases from 0.436 to 0.615. The stratified volume of the cold side decreased from 4.06 cm^3 to 3.67 cm^3, and the temperature difference between the stratified region and the outlet decreased from 1.21 K to 0.61 K.

On the other hand, the effectiveness increases from 0.576 to 0.597 as the inlet temperature difference between the inlet of the cold and hot side decreases from 30 K to 15 K due to the increase in the cold side. As a result, the stratified volume of the cold side decreases from 3.73 cm^3 to 3.64 cm^3, and the temperature difference between the stratified region and the outlet decreases from 1.18 K to 0.55 K. When the mass flow rate of the cold side increases from 0.03 kg/s to 0.12 kg/s, the difference between the maximum and minimum temperature at the dimensionless distance with 1D decreases from 0.72 K to 0.12 K. On the other hand, when the inlet temperature difference between the cold and hot sides increases from 15 K to 30 K, the difference between the maximum and the minimum temperature increases from 0.41 K to 0.79 K when the dimensionless distance is 1D. The non-uniformity of the outlet temperature of the plate heat exchanger is because the fluid having a non-uniform temperature in the merged part is not sufficiently mixed due to stratification. The increase in mass flow strengthens the diffusion of turbulence at the outlet pipe, shortening the dimensionless distance required to reach a uniform temperature at the outlet pipe.

Author Contributions: Conceptualization, H.C. and D.-w.O.; methodology G.L.; validation, G.L. and H.C.; formal analysis, J.H.; investigation, J.H. and G.L.; resources, J.H. and D.-w.O.; writing—original draft preparation, J.H. and H.C.; writing—review and editing, H.C. and D.-w.O.; supervision, H.C. All authors have read and agreed to the published version of the manuscript.

Funding: This work was supported by the Nuclear Safety Research Program through the Korea Foundation of Nuclear Safety (KOFONS) using the financial resource granted by the Nuclear Safety and Security Commission (NSSC) of the Republic of Korea (NO. 1805007).

Institutional Review Board Statement: Not applicable.

Informed Consent Statement: Not applicable.

Data Availability Statement: Not applicable.

Conflicts of Interest: The authors declare no conflict of interest. The funders had no role in the design of the study; in the collection, analyses, or interpretation of data; in the writing of the manuscript, or in the decision to publish the results.

Abbreviations

Nomenclature

A_l	Effective corrugated area (m^2)
A_{lp}	Projectred surface area (m^2)
b	Corrugation depth (m)
C	Heat capacity rate (W/K)
c_p	Specific heat (J/kg·K)
D_h	Hydrodynamic diameter (m)
D_p	Port diameter (m)
h	Heat transfer coefficient ($W/m^2 \cdot K$)
I	Turbulence intensity
k	Thermal conductivity (W/m·K)
L_p	Port to port length (m)
L_v	Chevron area length (m)
L_w	Port to port plate width (m)
$\dot{m}$	Mass flow rate (kg/s)
Nu	Nusselt number
Re	Reynolds number
Pr	Prandtl number
T	Temperature (K)
t	Thickness of the plate (m)
Q	Amount of heat transfer (W)

Greek Symbols

β	Ratio of velocity or temperature
$\overline{\beta}$	Average ratio of velocity or temperature
ε	Effectiveness
ϕ	Non-uniformity
μ	Viscosity (Pa·s)
ρ	Density (kg/m^3)

Subscript

avg	Average
c	Cold side
ch	Channel
h	Hot side
i	Inlet
max	Maximum
min	Minimum
o	Outlet
$pipe$	Pipe

References

1. Payambarpour, S.A.; Shokouhmand, H.; Ahmadi, M.H.; Assad, M.E.H.; Chen, L. Effect of wetness pattern on the fin-tube heat exchanger performance under partially wet-surface condition. *Therm. Sci. Eng. Prog.* **2020**, *19*, 100619. [CrossRef]
2. Payambarpour, S.A.; Nazari, M.A.; Ahmadi, M.H.; Chamkha, A.J. Effect of partially wet-surface condition on the performance of fin-tube heat exchanger. *Int. J. Numer. Methods Heat Fluid Flow* **2019**, *29*, 3938–3958. [CrossRef]
3. Hu, W.-L.; Ma, A.-J.; Guan, Y.; Cui, Z.-J.; Zhang, Y.-B.; Wang, J. Experimental Study of the Air Side Performance of Fin-and-Tube Heat Exchanger with Different Fin Material in Dehumidifying Conditions. *Energies* **2021**, *14*, 7030. [CrossRef]
4. Kim, D.-K. Comparison of optimal thermal performances of finned tube annuli with various fin shapes. *Int. J. Heat Mass Transf.* **2021**, *175*, 121402. [CrossRef]
5. Dinsing, N.; Schmitz, N.; Schubert, C.; Pfeifer, H. Development of an Efficient Modelling Approach for Fin-Type Heat-Exchangers in Self-Recuperative Burners. *Energies* **2021**, *14*, 6873. [CrossRef]
6. Goodarzi, M.; Amiri, A.; Goodarzi, M.S.; Safaei, M.R.; Karimipour, A.; Languri, E.M.; Dahari, M. Investigation of heat transfer and pressure drop of a counter flow corrugated plate heat exchanger using MWCNT based nanofluids. *Int. Commun. Heat Mass Transf.* **2015**, *66*, 172–179. [CrossRef]
7. Bahmani, M.H.; Sheikhzadeh, G.; Zarringhalam, M.; Akbari, O.A.; Alrashed, A.A.A.A.; Shabani, G.A.S.; Goodarzi, M. Investigation of turbulent heat transfer and nanofluid flow in a double pipe heat exchanger. *Adv. Powder Technol.* **2018**, *29*, 273–282. [CrossRef]
8. Cademartori, S.; Cravero, C.; Marini, M.; Marsano, D. CFD Simulation of the Slot Jet Impingement Heat Transfer Process and Application to a Temperature Control System for Galvanizing Line of Metal Band. *Appl. Sci.* **2021**, *11*, 1149. [CrossRef]
9. Huang, H.; Sun, T.; Zhang, G.; Li, D.; Wei, H. Evaluation of a developed SST k-ω turbulence model for the prediction of turbulent slot jet impingement heat transfer. *Int. J. Heat Mass Transf.* **2019**, *139*, 700–712. [CrossRef]
10. Hayes, A.M.; Khan, J.A.; Shaaban, A.H.; Spearing, I.G. The thermal modeling of a matrix heat exchanger using a porous medium and the thermal non-equilibrium model. *Int. J. Therm. Sci.* **2008**, *47*, 1306–1315. [CrossRef]
11. Wang, C.C.; Yang, K.S.; Tsai, J.S.; Chen, I.Y. Characteristics of flow distribution in compact parallel flow heat exchangers, part I: Typical inlet header. *Appl. Therm. Eng.* **2011**, *31*, 3226–3234. [CrossRef]
12. Wang, C.C.; Yang, K.S.; Tsai, J.S.; Chen, I.Y. Characteristics of flow distribution in compact parallel flow heat exchangers, part II: Modified inlet header. *Appl. Therm. Eng.* **2011**, *31*, 3235–3242. [CrossRef]
13. Huang, C.H.; Wang, C.H. The study on the improvement of system uniformity flow rate for U-type compact heat exchangers. *Int. J. Heat Mass Transf.* **2013**, *63*, 1–8. [CrossRef]
14. Said, S.A.M.; Ben-Mansour, R.; Habib, M.A.; Siddiqui, M.U. Reducing the flow mal-distribution in a heat exchanger. *Comput. Fluids* **2015**, *107*, 1–10. [CrossRef]
15. Guo, Z.Y.; Zhou, S.Q.; Li, Z.X.; Chen, L.G. Theoretical analysis and experimental confirmation of the uniformity principle of temperature difference field in heat exchanger. *Int. J. Heat Mass Transf.* **2002**, *45*, 2119–2127. [CrossRef]
16. Labbadlia, O.; Laribi, B.; Chetti, B.; Hendrick, P. Numerical study of the influence of tube arrangement on the flow distribution in the header of shell and tube heat exchangers. *Appl. Therm. Eng.* **2017**, *126*, 315–321. [CrossRef]

17. Wang, K.; Tu, X.C.; Bae, C.H.; Kim, H.B. Optimal design of porous baffle to improve the flow distribution in the tube-side inlet of a shell and tube heat exchanger. *Int. J. Heat Mass Transf.* **2015**, *80*, 865–872. [CrossRef]
18. Kim, M.-H.; Nguyen, V.T.; Im, S.; Jung, Y.; Choi, S.-R.; Kim, B.-J. Experimental Validation of Flow Uniformity Improvement by a Perforated Plate in the Heat Exchanger of SFR Steam Generator. *Energies* **2021**, *14*, 5846. [CrossRef]
19. Wen, J.; Li, Y.; Zhou, A.; Zhang, K.; Wang, J. PIV experimental investigation of entrance configuration on flow maldistribution in plate-fin heat exchanger. *Cryogenics* **2006**, *46*, 37–48. [CrossRef]
20. Wang, S.; Li, Y.; Wen, J.; Ma, Y. Experimental investigation of header configuration on two-phase flow distribution in plate-fin heat exchanger. *Int. Commun. Heat Mass Transf.* **2010**, *37*, 116–120. [CrossRef]
21. Zhang, Z.; Mehendale, S.; Tian, J.J.; Li, Y.Z. Experimental investigation of distributor configuration on flow maldistribution in plate-fin heat exchangers. *Appl. Therm. Eng.* **2015**, *85*, 111–123. [CrossRef]
22. Yang, H.; Wen, J.; Gu, X.; Liu, Y.; Wang, S.; Cai, W.; Li, Y. A mathematical model for flow maldistribution study in a parallel plate-fin heat exchanger. *Appl. Therm. Eng.* **2017**, *121*, 462–472. [CrossRef]
23. Jin, S.; Hrnjak, P. Effect of end plates on heat transfer of plate heat exchanger. *Int. J. Heat Mass Transf.* **2017**, *108*, 740–748. [CrossRef]
24. Navarro-Peris, E.; Alvarez-Piñeiro, L.; Schnabel, L.; Corberan, J.M. Refrigerant maldistribution in brazed plate heat exchanger evaporators. Part B: Analysis of the influence of maldistribution on the evaporator performance. *Int. J. Refrig.* **2021**, *131*, 312–321. [CrossRef]
25. Navarro-Peris, E.; Alvarez-Piñeiro, L.; Albaladejo, P.; Schnabel, L.; Corberan, J.M. Refrigerant maldistribution in brazed plate heat exchanger evaporators. Part A: Testing campaign and experimental results. *Int. J. Refrig.* **2021**, *131*, 119–128. [CrossRef]
26. Bobbili, P.R.; Sunden, B.; Das, S.K. An experimental investigation of the port flow maldistribution in small and large plate package heat exchangers. *Appl. Therm. Eng.* **2006**, *26*, 1919–1926. [CrossRef]
27. Bassiouny, M.K.; Martin, H. Flow distribution and pressure drop in plate heat exchangers—I U-type arrangement. *Chem. Eng. Sci.* **1984**, *39*, 693–700. [CrossRef]
28. Rao, B.P.; Das, S.K. An Experimental Study on the Influence of Flow Maldistribution on the Pressure Drop Across a Plate Heat Exchanger. *J. Fluids Eng.* **2004**, *126*, 680–691. [CrossRef]
29. Tereda, F.A.; Srihari, N.; Sunden, B.; Das, S.K. Experimental Investigation on Port-to-Channel Flow Maldistribution in Plate Heat Exchangers. *Heat Transf. Eng.* **2007**, *28*, 435–443. [CrossRef]
30. Rao, B.P.; Das, S.K. Effect of Flow Distribution to the Channels on the Thermal Performance of the Multipass Plate Heat Exchangers. *Heat Transf. Eng.* **2004**, *25*, 48–59. [CrossRef]
31. Brenk, A.; Pluszka, P.; Malecha, Z. Numerical Study of Flow Maldistribution in Multi-Plate Heat Exchangers Based on Robust 2D Model. *Energies* **2018**, *11*, 3121. [CrossRef]
32. Wang, Y.-N.; Lee, J.-P.; Park, M.-H.; Jin, B.-J.; Yun, T.-J.; Song, Y.-H.; Kim, I.-S. A study on 3D numerical model for plate heat exchanger. *Procedia Eng.* **2017**, *174*, 188–194. [CrossRef]
33. Yadav, V.; Baghel, K.; Kumar, R.; Kadam, S.T. Numerical investigation of heat transfer in extended surface microchannels. *Int. J. Heat Mass Transf.* **2016**, *93*, 612–622. [CrossRef]
34. Gulenoglu, C.; Akturk, F.; Aradag, S.; Sezer Uzol, N.; Kakac, S. Experimental comparison of performances of three different plates for gasketed plate heat exchangers. *Int. J. Therm. Sci.* **2014**, *75*, 249–256. [CrossRef]
35. Jurtz, N.; Kraume, M.; Wehinger, G.D. Advances in fixed-bed reactor modeling using particle-resolved computational fluid dynamics (CFD). *Rev. Chem. Eng.* **2019**, *35*, 139–190. [CrossRef]